Response function of a moving contact line

H. Perrin,[1,*] D. Belardinelli,[2,†] M. Sbragaglia,[2,‡] and B. Andreotti[1,§]
[1]*Laboratoire de Physique Statistique, UMR 8550 ENS-CNRS, Univ. Paris-Diderot, 24 rue Lhomond, 75005 Paris, France*
[2]*Department of Physics and INFN, University of Rome "Tor Vergata," Via della Ricerca Scientifica 1, 00133 Rome, Italy*

(Received 5 August 2017; published 9 April 2018)

The hydrodynamics of a liquid-vapor interface in contact with a heterogeneous surface is largely impacted by the presence of defects at the smaller scales. Such defects introduce morphological disturbances on the contact line and ultimately determine the force exerted on the wedge of liquid in contact with the surface. From the mathematical point of view, defects introduce perturbation modes, whose space-time evolution is governed by the interfacial hydrodynamic equations of the contact line. In this paper we derive the response function of the contact line to such generic perturbations. The contact line response may be used to design simplified one-dimensional time-dependent models accounting for the complexity of interfacial flows coupled to nanoscale defects, yet offering a more tractable mathematical framework to explore contact line motion through a disordered energy landscape.

DOI: 10.1103/PhysRevFluids.3.044001

I. INTRODUCTION

The dynamics of a liquid-gas-solid interface (contact line) on heterogeneous substrates is a complex problem at the crossroads between physics, chemistry, and engineering. The physical description of the problem in the ideal situation of a flat homogeneous solid is well understood at macroscales [1,2]; however, understanding the influence of roughness and/or of chemical defects at smaller scales remains a challenging task, largely open despite recent progress [3–7]. Such a problem is of both fundamental and practical importance, with a variety of examples ranging across scales. One may cite problems involving microscale roughness, such as dynamic spreading [8,9], cooling applications [10], ink-jet printing of electronic circuits [11–14], droplet control [15–18], patterning of substrates [19], deposition [20], and adhesion of reticulated polymers [21]. At even smaller scales, one may mention contact line morphology and pinning on colloids [22–28], nanodroplets on structured surfaces [29–31], spreading [32,33] and drainage [34,35] at nanoscales, hysteresis caused by nanodefects [36], and metastability of wetting states [37,38].

A paradigmatic setup for dynamic contact line flows is the deposition of a thin liquid layer on a solid surface withdrawn from a liquid reservoir [39–42]. The force balance exerted on a wedge of liquid along the contact line under the influence of the solid is macroscopically parametrized by the surface tensions of the liquid-vapor (γ), solid-liquid (γ_{sl}), and solid-vapor interfaces (γ_{sv}): as a direct consequence of the intermolecular forces, they provide excess free energies associated with the interfaces and combine at equilibrium to provide the contact angle θ_Y made by the liquid-vapor

*hugo.perrin@espci.fr
†belardinelli@roma2.infn.it
‡sbragaglia@roma2.infn.it
§andreotti@lps.ens.fr

interface with respect to the solid, i.e., the celebrated Young's law [2]

$$\gamma \cos\theta_Y = \gamma_{\mathrm{sv}} - \gamma_{\mathrm{sl}}.$$

Substrate heterogeneities are therefore naturally described in terms of a frozen, disordered surface energy landscape. This frozen energy landscape constitutes the first difficulty of the problem: the force of solid origin exerted on the fluid depends on the location of the contact line. As weak interactions quickly decay with the distance between molecules, the contact angle locally made by the liquid is selected at a molecular scale [43,44], and Young's law therefore acts as a boundary condition for the mesoscopic interface, which encodes possible finite thickness effects as those standardly described by a disjoining pressure [45,46]. Notice that we use the term "mesoscopic" to refer to the intermediate range of scales between molecular scales (where processes explicitly depend on molecular size) and macroscopic, where gravity or an outer boundary condition matters.

The flow resulting from the contact line motion must be described by interfacial hydrodynamics, which immediately reveals the second difficulty of the problem: as a contact line is a geometrical singularity, the corner flow [47] presents a viscous stress that tends to diverge at the contact line but remains finite due to some molecular scale regularization process. Viscous dissipation of energy takes place at all length scales between the molecular scale and the size of the meniscus [47]. This yields a total dissipation that is integrable neither at the singularity nor at infinity, and the problem requires a cutoff at both the small and large scales. Typically, these cutoffs appear at a molecular scale ($\sim 10^{-9}$ m), and at the scale of the capillary length ℓ_γ ($\sim 10^{-3}$ m). Each of the decades between the microscopic scale and the macroscopic scale contributes to the viscous dissipation, revealing the intrinsic multiscale character of wetting flows. These features of moving contact lines were first appreciated by Hue and Scriven [47], who analytically solved the flow in a perfect wedge using similarity solutions. The equations considerably simplify in the limit of small interfacial slopes and curvatures, i.e., in the lubrication limit [48]. In such a limit, the relevant dynamical quantities reduce to the thickness h of liquid from the solid to the interface and the average velocity $\vec{U}$ parallel to the solid (plate).

The importance of physico-chemical heterogeneities at small scales together with the necessity to include a regularization mechanism for the contact line problem also sets a compelling case for the understanding of the role of thermal fluctuations. Indeed, at nanoscales, the strength of thermal fluctuations becomes comparable to that of surface tension, hence fluctuations may trigger activated dynamics across defects [49]. From the point of view of macroscopic interfacial hydrodynamics, thermal fluctuations may be embedded in a continuum description of the contact line flows based on fluctuating hydrodynamics [50–52], i.e., the equations of hydrodynamics where the viscous stress tensor is supplemented with a stochastic contribution accounting for the random motion of molecules at small scales. Different studies have been proposed in the literature, based on the lubrication approximation [32,33,53–55]. In this framework, boundary conditions are typically needed to account for the impenetrable nature of the boundaries [33,56]; capillary waves, in turn, may be affected by the restrictions imposed by the boundaries [57–59], resulting in morphological changes of the average profile on the scale of the thermal length. A semiphenomenological (coarse-grained) parameter may be introduced [54] to account for the affinity of the contact line with the substrate, and exact calculations may be performed to predict the shape of the profiles close to the wall. However, the microscopic derivation of this parameter requires a suitable matching with an inner description, possibly including the details of the heterogeneities. This leaves us with a third difficulty, i.e., rationalizing a framework for a fluctuating contact line problem coupled to a precise realization of nanoscale defects. Placing the effects of thermal fluctuations on the full (time-dependent) contact line problem with an heterogeneous realization of defects on a surface looks an hard task. This is not even required if we are not interested in all the details of the contact line profile [60] but rather want to predict and control the activated hopping of its average position. A first step towards this approach consists in the systematic derivation of the *response function*, i.e., the (linear) relation between the displacement and the force exerted along the contact line profile in the presence of heterogeneities. This is precisely the purpose of this article. Once the response function is known, one can write a

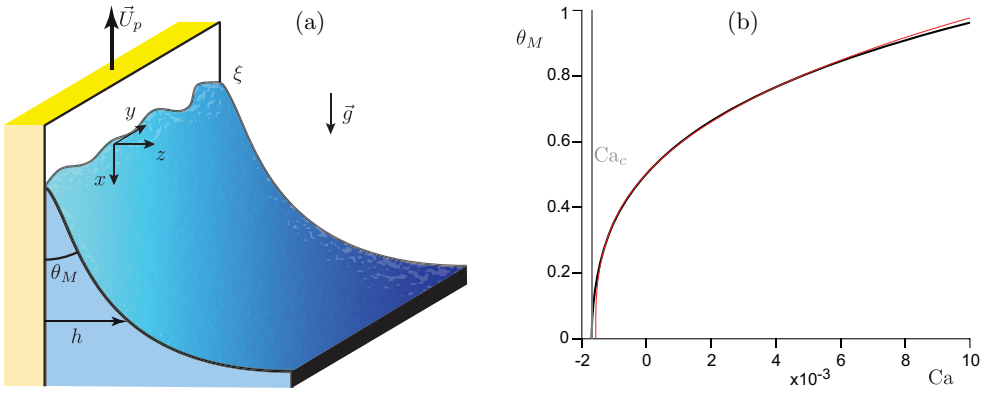

FIG. 1. (a) The response function of the dynamic contact line is determined in the dip-coating geometry. A vertical plate is plunged ($U_p > 0$) or withdrawn ($U_p < 0$, as in the figure) from a bath at the velocity $\vec{U}_p = U_p \vec{e}_x$. The contact line profile is denoted by ξ. The bath, far from the plate, is at equilibrium. Its asymptotic profile when approaching the plate resembles that of a static bath and would join the plate, if prolonged, at an angle θ_M called the macroscopic contact angle [see Eq. (12)]. (b) Relation between the apparent contact angle θ_M and the capillary number $\mathrm{Ca} = \eta U_p/\gamma$ determined using a slip length $\ell_s = 2.5\times 10^{-6}\,\ell_\gamma$ and a microscopic contact angle $\theta_0 = 0.5$ rad, corresponding to about 28.6°. Here $\mathrm{Ca_c}$ is the threshold capillary number below which a liquid film is entrained on the plate and corresponds to $\theta_M = 0$. The thin red line is the approximation by the Cox-Voinov formula (13).

Langevin equation and possibly introduce a thermal noise term in a more tractable way [61]. To obtain the response function, we will assume that disturbances introduced by defects are small and can still be described in the hydrodynamic framework as elastic perturbations [1,2,60,62]. We will then concentrate on the evolution equations of such perturbations in the lubrication limit for the well-known dip-coating setup [39–42], consisting of a plate withdrawal from a bath at a constant velocity. The response function will be fully characterized at changing wave numbers and frequency of the boundary perturbations.

The paper is organized as follows: Sec. II deals with the theoretical framework utilized in the present paper; the properties of the dynamical base state are reviewed in Sec. III, and the dynamical equations for the perturbations are the subject of Sec, IV; the characterization of the response function is found in Sec. V. Some concluding remarks and perspectives are offered in Sec. VI.

II. THEORETICAL FRAMEWORK

Our aim here is to describe the contact line motion on a heterogeneous substrate. We consider the seminal dip-coating geometry in which a plate is plunged ($U_p > 0$) or withdrawn ($U_p < 0$) from a bath at a constant velocity $\vec{U}_p$ [39–42] [see Fig. 1(a)]. The liquid has a mass density ρ, a viscosity η, and a surface tension γ. The coordinates are x and y along the plate, with x going from the contact line to the bath, and z normal to the plate, while t is the instant of time. The plate velocity U_p can be rescaled by the typical velocity γ/η for which viscous stress and capillarity are of the same order of magnitude:

$$\mathrm{Ca} = \frac{\eta U_p}{\gamma}.$$

Gravity, whose acceleration is g, fixes the outer length scale of the problem, the capillary length

$$\ell_\gamma = \sqrt{\frac{\gamma}{\rho g}}.$$

To determine the response function of a dynamic contact line, we adopt a continuous description valid from just above the molecular scale—the typical range of intermolecular interactions and of slip effects—up to the outer length scale fixed by ℓ_γ. Consistently with this description, surface heterogeneities can be encoded, whatever their nature and length scale, into a single field $T_Y(x,y)$ which gives the contact angle when the contact line is at the location (x,y). We emphasize that this does not constitute a limit of the model, which can be used to describe nanometer scale defects provided a clear definition of $T_Y(x,y)$. The density functional theory (DFT) is the proper way to model capillarity at the nanometer scale [63]. A convenient, controlled approximation of DFT is to push this theory in the limit of a sharp interface [43,64–67]. The disjoining pressure approach can be thought of as a further approximation valid in the limit of almost flat interfaces [66]. They all in common lead to the selection of a constant angle at a scale slightly larger than the molecular scale, which must be equal to Young's angle when the substrate is homogeneous. $T_Y(x,y)$ characterizes the angle of the outer solution, seen from the molecular scale. It therefore includes possible nonlocal effects taking place at the molecular scale in an effective way. DFT and its approximations must therefore be considered as ways to compute $T_Y(x,y)$ from a map giving the atomistic composition of the surface. It is important to note, though, that $T_Y(x,y)$ is the most accessible quantity from an experimental perspective. Alternative formulations have been proposed to include correction terms to the macroscopic free energy, in order to include molecular scale effects: curvature-dependent surface tension [68–72] and line tension [73–75]. As they critically rely on the definition of the interface location, both effects lead to conflicting results on their magnitude and even their sign [76–78]. The literature has reached a consensual agreement that they can fairly be ignored above few molecular scales [66,72]. The only true limit of our calculation therefore results from the linearization of a dynamical equation around a flat contact line, which, in addition, implies that line tension can be ignored. In summary, from the macroscopic perspective, the boundary condition is the contact angle $\theta_Y(y,t)$ along the contact line profile that we decompose as $x = \xi_0 + \xi(y,t)$. ξ_0 is the average position over space and time (or over realizations), and ξ the fluctuating part in space and time. On the one hand, the angle of the liquid interface along the contact line $\theta_Y(y,t)$ results from a frozen landscape $T_Y(x,y)$ such that it corresponds to the value of the frozen landscape at the location of the contact line: $\theta_Y(y,t) = T_Y(\xi_0 + \xi(y,t), y)$. The contact angle profile is determined by the contact line position, which itself depends on the contact angle distribution. On the other hand, the flow and therefore the evolution of the contact line position is entirely driven by $\theta_Y(y,t)$, as being the boundary condition of the dynamic liquid interface. We can therefore solve for the hydrodynamics problem, assuming that $\theta_Y(y,t)$ is known in advance, and determine the evolution of $\xi(y,t)$. The two parts of the problem, namely, the selection of $\theta_Y(y,t)$ by the value of the frozen landscape at the location of the contact line and the hydrodynamics driven by $\theta_Y(y,t)$, can therefore be treated separately and coupled afterward.

We use the lubrication approximation of Navier-Stokes [48] and linearize the solution with respect to the perturbation:

$$F(y,t) = \gamma[\cos\theta_Y(y,t) - \cos\theta_0], \tag{1}$$

where $\cos\theta_0$ is the average over space and time (or over realizations in an unsteady statistical process) of $\cos\theta_Y$, which is evaluated from the frozen field $T_Y(x,y)$ along the contact line. The value of $\cos\theta_0$ therefore results from the dynamics but the hydrodynamic problem can be treated, parametrized by θ_0, ignoring its actual value. We wish to find the position, knowing the boundary condition $\theta_Y(y,t)$. For this, we perform the double Fourier transform of the contact line profile $\xi(y,t)$ over space and over time:

$$\hat{\xi}(q,\omega) = \int_{-\infty}^{+\infty} dt \int dy\, e^{-j\omega t - jqy}\xi(y,t).$$

The integral in y extends over the whole space or over the periodicity domain. $\hat{\xi}(q,\omega)$ is linearly related to the force disturbance Fourier transform:

$$\gamma \mathcal{C}(q,\omega)\hat{\xi}(q,\omega) = \hat{F}(q,\omega), \tag{2}$$

where the *response function* $\mathcal{C}(q,\omega)$, which is homogeneous to the inverse of a length, is calculated from hydrodynamics for any mode q. For a small variation θ_1 of the contact angle to its space and time average one can linearize the force disturbance as $\cos(\theta_0+\theta_1)-\cos\theta_0 \simeq -\sin\theta_0\,\theta_1$; hence from (1) and (2) we can write

$$\mathcal{C}(q,\omega)\hat{\xi}(q,\omega) \simeq -\sin\theta_0\,\hat{\theta}_1(q,\omega), \tag{3}$$

which relates the contact angle variation and the contact line disturbance through the response function. The average position of the contact line ξ_0 over space and time has been singled out, which is actually a function of θ_0 and of the capillary number Ca. Note that the problem does not need to be in a statistically steady state: θ_0 and Ca may vary as a function of time, in which case ξ_0 adapts consequently (more details are given in Sec. V C). Further note that θ_0 is ultimately a function of Ca and of the statistical properties of the frozen disorder T_Y, due to the fact that it results from an average along the contact line. The sampling of the energy landscape is therefore biased. Similarly, Eq. (2) is the dynamical equation for the contact line fluctuations, as F is a function of ξ through the reading of the energy landscape. When computing the response function, the angular frequency ω is rescaled by $\gamma/\eta\ell_\gamma$ and will be noted as

$$\Omega \equiv \frac{\eta\ell_\gamma}{\gamma}\omega.$$

III. DYNAMICAL BASE STATE

The lubrication equations with a Navier slip boundary condition read as [48]

$$\partial_t h + \vec{\nabla}\cdot(h\,\vec{U}) = 0, \tag{4}$$

$$\gamma\vec{\nabla}\kappa + \rho g\vec{e}_x + \frac{3\eta(U_p\vec{e}_x - \vec{U})}{h(h+3\ell_s)} = \vec{0}, \tag{5}$$

where ℓ_s is the slip length. They constitute a controlled approximation of the Stokes equations under the condition of small slope and small product of the curvature κ by the thickness h. Here the surface is located at $z = h(x,y,t)$, while $\vec{\nabla} = \vec{e}_x\partial_x + \vec{e}_y\partial_y$ is the gradient operator along the plate, $\vec{e}_i$ being the unit vector of the ith coordinate, $\vec{U}(x,y,t) = \vec{e}_x U_x(x,y,t) + \vec{e}_y U_y(x,y,t)$ is the velocity along the plate averaged over z:

$$\vec{U} = \frac{1}{h}\int_0^h \vec{u}\,dz,$$

$\vec{u}(x,y,z,t)$ being the true hydrodynamic velocity along the plate. The continuity equation (4) expresses the conservation of mass for the problem at hand, and the quantity $h\,\vec{U}$ is the flux vector along the plate. The curvature $\kappa(x,y,t)$ of the surface, appearing in the force balance Eq. (5), is given by

$$\kappa = \frac{(1+\partial_y h^2)\partial_{xx}h + (1+\partial_x h^2)\partial_{yy}h - 2\partial_x h\,\partial_y h\,\partial_{xy}h}{(1+\partial_x h^2+\partial_y h^2)^{3/2}} \tag{6}$$

and is related to the pressure $P(x,y,t)$ by the Laplace formula $P = -\gamma\kappa$. We introduce γ/η as a unit velocity and ℓ_γ as a unit length for spatial coordinates x and y and for the thickness h. Dimensionless variables will be noted in the same way as the variables themselves, except U_p, which becomes Ca. When needed, we will give back expressions with their dimensions, mentioning it explicitly. The

lubrication equations read

$$\partial_t h + \vec{\nabla} \cdot (h\,\vec{U}) = 0, \tag{7}$$

$$\vec{\nabla}\kappa + \vec{e}_x + \frac{3(\mathrm{Ca}\,\vec{e}_x - \vec{U})}{h(h+3\ell_s)} = \vec{0}. \tag{8}$$

The formulation of the boundary conditions for the dynamical problem requires a further discussion, and we postpone it to Sec. IV. Let $h(x,y,t) = h_0(x)$ be the steady transversely invariant surface profile, for which the curvature $\kappa(x,y,t) = \kappa_0(x)$ reduces to [use of a prime ($'$) means derivation with respect to x]

$$\kappa_0 = \frac{h_0''}{\left(1+h_0'^2\right)^{3/2}}.$$

This steady and transversely invariant liquid interface profile constitutes the base state, noted with the subscript 0. From the continuity equation and condition of zero flux at the contact line we get $\vec{U}(x,y,t) = \vec{U}_0(x) = \vec{0}$. The lubrication equations reduce to

$$\kappa_0' + 1 + \frac{3\mathrm{Ca}}{h_0(h_0+3\ell_s)} = 0.$$

Regardless of the convention for ξ_0, it is convenient to choose the location of the contact line for the steady transversely invariant case as $x = 0$. The boundary conditions at the plate are then

$$h_0(0) = 0,$$
$$h_0'(0) = \tan\theta_0.$$

By starting from the boundary conditions for h_0 and h_0' at $x = 0$, one can find the asymptotics of the base state at the plate by solving recursively the system

$$h_0'' = \left(1+h_0'^2\right)^{3/2}\kappa_0,$$
$$\kappa_0' = -1 - \frac{3\mathrm{Ca}}{h_0(h_0+3\ell_s)}.$$

We get the following asymptotics of the base state at the plate, for $x \to 0$:

$$h_0(x) = t_0 x - \frac{\mathrm{Ca}\left(1+t_0^2\right)^{3/2}}{2\ell_s t_0}x^2\ln\left(\frac{x}{\ell}\right) + \frac{3\mathrm{Ca}\left(1+t_0^2\right)^{3/2}}{4\ell_s t_0}x^2 + O(x^3\ln^2 x), \tag{9}$$

$$h_0'(x) = t_0 - \frac{\mathrm{Ca}\left(1+t_0^2\right)^{3/2}}{\ell_s t_0}x\ln\left(\frac{x}{\ell}\right) + \frac{\mathrm{Ca}\left(1+t_0^2\right)^{3/2}}{\ell_s t_0}x + O(x^2\ln^2 x), \tag{10}$$

$$\kappa_0(x) = -\frac{\mathrm{Ca}}{\ell_s t_0}\ln\left(\frac{x}{\ell}\right) - \frac{\mathrm{Ca}^2\left(1+t_0^2\right)^{3/2}}{2\ell_s^2 t_0^3}x\ln\left(\frac{x}{\ell}\right) - \left[1 - \frac{\mathrm{Ca}}{3\ell_s^2} - \frac{5\mathrm{Ca}^2\left(1+t_0^2\right)^{3/2}}{4\ell_s^2 t_0^3}\right]x + O(x^2\ln^2 x), \tag{11}$$

where $t_0 = \tan\theta_0$, for shortness, while ℓ is a free parameter, adjusted by shooting to match the bath. Note that, in practice, it is convenient to introduce the quantity $\mathrm{Ca}\ln\ell$ rather than ℓ itself.

The concept of macroscopic contact angle has long been a source of confusion in the literature. The proper way of defining it is to start from the asymptotics at the bath, which is exactly that of a static bath at equilibrium. The constant M (see below), though, which describes the exponential departure from the flat bath (considering x vs h_0) depends on the dynamic solution between the scale of the slip length and that of the capillary length. The static-like asymptotics at the bath can be prolonged and

would join the plate at an angle, which is by definition the macroscopic angle θ_M. The macroscopic contact angle is therefore not a true interface angle but is defined by asymptotic matching of the solution coming from the dynamical range of scales with an outer, static bath solution. The position at which the static bath interface would join the plate is almost the same as the true contact line position. In practice, the macroscopic angle θ_M can therefore be defined from the altitude δ of the contact line using the following static relation [50]:

$$\delta = \sqrt{2(1-\sin\theta_M)}\,\ell_\gamma. \tag{12}$$

The difference between the capillary forces $\gamma\cos\theta_M$ and $\gamma\cos\theta_0$ at macroscopic and microscopic scales results from the viscous force integrated along the plate, between the inner and outer scales. A useful approximation is that provided by the Cox-Voinov derivation [79], which is a particular solution of the lubrication equations matched macroscopically to a vanishing curvature interface. It is derived at the linear order in angle but turns out to provide an excellent nonlinear fit of the actual solution [see Fig. 1(b)], for uncontrolled reasons:

$$\theta_M^3 \sim \theta_0^3 + 9\mathrm{Ca}\ln\left(\frac{\alpha\ell_\gamma}{3\ell_s}\right), \tag{13}$$

where $\alpha \simeq 0.02$ is independent, in first approximation, of the contact angle. The interested reader may find the correct asymptotic expansion in Refs. [39–42]. Equation (12) is an exact result for the static bath, as the static profile decays exponentially as $\delta - x \sim e^{-h}$ at large heights h. We therefore look for the following asymptotics at the bath for $x \to \delta$:

$$h_0(x) \sim -\ln\left(\frac{\delta-x}{M}\right), \tag{14}$$

$$h_0'(x) \sim \frac{1}{\delta-x}, \tag{15}$$

$$\kappa_0(x) \sim \delta - x, \tag{16}$$

where M is a free parameter, adjusted by shooting to match the contact line. Note that δ is the distance between the average contact line and the bath.

IV. LINEARIZED EQUATIONS

We linearize Eqs. (6)–(8) about the basic profile $h_0(x)$, writing the profile as a combination of the base state and a small disturbance, noted with subscript 1, oscillating in time at frequency Ω and modulated spatially at wave number q:

$$h(x,y,t) = h_0(x) + h_1(x)\,e^{j\Omega t+jqy}, \tag{17}$$

$$\kappa(x,y,t) = \kappa_0(x) + \kappa_1(x)\,e^{j\Omega t+jqy}, \tag{18}$$

$$U_x(x,y,t) = u_1(x)\,e^{j\Omega t+jqy}, \tag{19}$$

$$U_y(x,y,t) = v_1(x)\,e^{j\Omega t+jqy}. \tag{20}$$

The curvature linearizes into

$$\kappa_1 = -\frac{q^2h_1}{\left(1+h_0'^2\right)^{1/2}} + \frac{h_1''}{\left(1+h_0'^2\right)^{3/2}} - \frac{3\kappa_0h_0'h_1'}{1+h_0'^2}.$$

From the y component of Eq. (8), one can eliminate v_1 in terms of κ_1, as

$$v_1 = \tfrac{1}{3}jqh_0(h_0+3\ell_s)\,\kappa_1.$$

It is convenient to introduce the variable

$$\mathcal{F}_1(x) = h_0(x)u_1(x),$$

which represents the flux in the x direction at first order (the zeroth order flux being zero). We get, from the linearized lubrication equations about the base state, the differential equations obeyed by the disturbed liquid interface [80]:

$$h_1'' = \left(1 + h_0'^2\right)q^2 h_1 + 3\left(1 + h_0'^2\right)^{1/2}\kappa_0 h_0' h_1' + \left(1 + h_0'^2\right)^{3/2}\kappa_1, \tag{21}$$

$$\kappa_1' = \frac{3\mathrm{Ca}(2h_0 + 3\ell_s)}{h_0^2(h_0 + 3\ell_s)^2}h_1 + \frac{3}{h_0^2(h_0 + 3\ell_s)}\mathcal{F}_1, \tag{22}$$

$$\mathcal{F}_1' = -j\Omega h_1 + \frac{h_0^2(h_0 + 3\ell_s)q^2}{3}\kappa_1. \tag{23}$$

Defining the quadrivector $\mathcal{X}$ as

$$\mathcal{X} = \begin{pmatrix} h_1 \\ h_1' \\ \kappa_1 \\ \mathcal{F}_1 \end{pmatrix},$$

one can rewrite the linearized equations (21)–(23) as [80]

$$\frac{d\mathcal{X}}{dx} = \mathcal{M}\mathcal{X}, \tag{24}$$

where

$$\mathcal{M} = \begin{pmatrix} 0 & 1 & 0 & 0 \\ \left(1 + h_0'^2\right)q^2 & 3\left(1 + h_0'^2\right)^{1/2}\kappa_0 h_0' & \left(1 + h_0'^2\right)^{3/2} & 0 \\ \frac{3\mathrm{Ca}(2h_0+3\ell_s)}{h_0^2(h_0+3\ell_s)^2} & 0 & 0 & \frac{3}{h_0^2(h_0+3\ell_s)} \\ -j\Omega & 0 & \frac{h_0^2(h_0+3\ell_s)q^2}{3} & 0 \end{pmatrix}.$$

There are many formulations that are equivalent at the linear order but that are differently accurate at the nonlinear order. In particular the exact solution of the problem exactly reduce to the solution of the linear problem at the linear order. In the present case we get (see the Appendix)

$$h_1(0) = -\tan\theta_0, \tag{25}$$

$$\lim_{x\to 0}[h_1'(x) + h_0''(x)] = -\frac{1 + \tan^2\theta_0}{\sin\theta_0}\mathcal{C}, \tag{26}$$

$$\mathcal{F}_1(0) = 0. \tag{27}$$

Note that $h_0''(x)$ diverges logarithmically as $h_0''(x) \sim -\frac{\mathrm{Ca}(1+\tan^2\theta_0)^{3/2}}{\ell_s \tan\theta_0}\ln\left(\frac{x}{\ell}\right)$ at $x = 0$, which explains the formulation of (26) with the limit. Here $\mathcal{C}$ is the response function, expressing the ratio between the disturbance of the forcing $\cos\theta_Y - \cos\theta_0$ and the disturbance on contact line position.

We now wish to derive the general asymptotics at the plate, to determine which of them are consistent with the boundary conditions in order to perform a numerical integration. We use for the base state the approximations (9)–(11). We then find the asymptotics of the perturbations for $x \to 0$ by solving recursively the resulting approximated system (24). As explained in the Appendix, we

get the following three physically acceptable independent asymptotics:

$$\mathcal{X}_h \sim \begin{pmatrix} 1 \\ -\frac{\mathrm{Ca}}{\ell_s \sin^2\theta_0 \cos\theta_0} \ln\left(\frac{x}{\ell}\right) \\ -\frac{\mathrm{Ca}}{\ell_s \tan^2\theta_0} x^{-1} \\ -\frac{q^2\mathrm{Ca}}{2} x^2 \end{pmatrix} - j\Omega \begin{pmatrix} \frac{1}{2\ell_s \sin^2\theta_0 \cos\theta_0} x^2 \ln\left(\frac{x}{\ell}\right) \\ \frac{1}{\ell_s \sin^2\theta_0 \cos\theta_0} x \ln\left(\frac{x}{\ell}\right) \\ \frac{1}{\ell_s \tan^2\theta_0} \ln\left(\frac{x}{\ell}\right) \\ x \end{pmatrix},$$

$$\mathcal{X}_\theta \sim \begin{pmatrix} x \\ 1 \\ \frac{\mathrm{Ca}}{\ell_s \tan^2\theta_0} \ln\left(\frac{x}{\ell}\right) \\ \frac{q^2\mathrm{Ca}}{3} x^3 \ln\left(\frac{x}{\ell}\right) \end{pmatrix} - j\Omega \begin{pmatrix} 0 \\ 0 \\ 0 \\ \frac{1}{2}x^2 \end{pmatrix}, \quad \mathcal{X}_\kappa \sim \begin{pmatrix} \frac{1}{2\cos^3\theta_0} x^2 \\ \frac{1}{\cos^3\theta_0} x \\ 1 \\ \frac{q^2\ell_s \tan^2\theta_0}{3} x^3 \end{pmatrix} - j\Omega \begin{pmatrix} 0 \\ 0 \\ 0 \\ \frac{1}{6\cos^3\theta_0} x^3 \end{pmatrix}.$$

So we must start the numerical integration with[1]

$$\mathcal{X} = -\tan\theta_0 \mathcal{X}_h - \frac{(1+\tan^2\theta_0)^{3/2}}{\tan\theta_0} \mathcal{C}\mathcal{X}_\theta + K\mathcal{X}_\kappa, \tag{28}$$

which satisfies the boundary conditions at the plate. The response function $\mathcal{C}$ appears in the asymptotics (28), together with another constant K. Both $\mathcal{C}$ and K must be chosen with a proper matching with the asymptotics at the bath.

The system (24) with the base state approximated by (14)–(16) reads

$$\mathcal{F}_1' = -j\Omega h_1 - \frac{q^2}{3\ln^3\left(\frac{\delta - x}{M}\right)} \kappa_1, \tag{29}$$

$$\kappa_1' = -\frac{6\mathrm{Ca}}{\ln^3\left(\frac{\delta - x}{M}\right)} h_1 - \frac{3}{\ln^3\left(\frac{\delta - x}{M}\right)} \mathcal{F}_1, \tag{30}$$

$$h_1'' = \frac{q^2}{(\delta - x)^2} h_1 + \frac{3}{\delta - x} h_1' + \frac{1}{(\delta - x)^3} \kappa_1. \tag{31}$$

These equations admit four asymptotics, among which two lead to a divergence of h_1 as $(\delta - x)^{-1}$ and $(\delta - x)^{-2}$, respectively. The two admissible asymptotics lead to a finite value of h_1 (convergence as $1/\ln^2[(\delta - x)/M]$ to zero and to a nonvanishing constant). As a simple criterion, we retain that $(\delta - x)h_1'$ tends to 0 for the two admissible solutions, as $1/\ln^3[(\delta - x)/M]$, but diverges for the two asymptotics that must be rejected, as $(\delta - x)^{-1}$ and $(\delta - x)^{-2}$, respectively. Furthermore, the curvature κ_1 of the two admissible solutions tends to 0 as $(\delta - x)/\ln^3[(\delta - x)/M]$ while one asymptotics that must be rejected tends to a constant and the other diverges as $(\delta - x)^{-1}/\ln^3[(\delta - x)/M]$. The specific feature of the acceptable asymptotics is the vanishing value of both $(\delta - x)h_1'$ and κ_1. We therefore use this property in the numerics to solve the superposition principle, without using explicitly the asymptotics.

To summarize, let us briefly recall the main steps of our analysis up to this point. After linearizing the interfacial equations of hydrodynamics, we have considered the evolution equations for the perturbation modes [cf. Eq. (17)]. These enabled us to determine the asymptotics at the plate [cf. Eq. (28)] as well as the asymptotics at the bath [cf. Eq. (29)]. In the asymptotics at the plate we have identified the response function $\mathcal{C}$: this must be computed in order that the asymptotics at the bath confirm the boundary conditions. This selection is carried out numerically [80]. In the next section

[1]When combined, all the asymptotics should be computed at the same order in x component per component; see the Appendix for details.

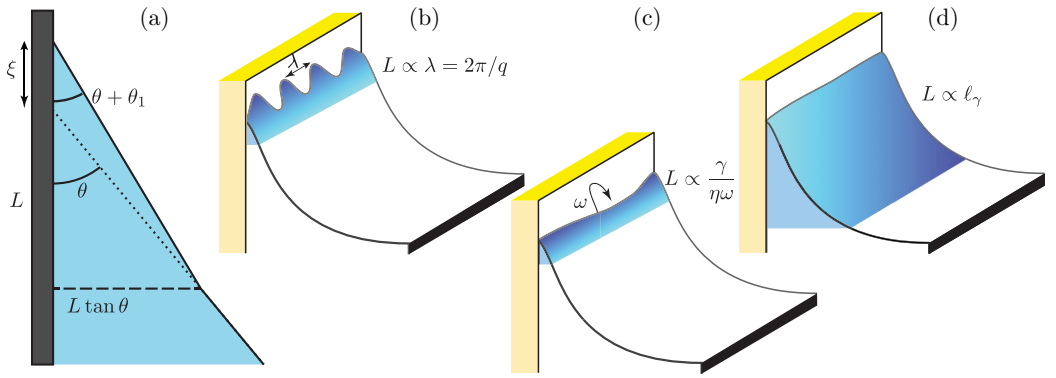

FIG. 2. (a) Schematic of the geometrical model relating the response function to the penetration length L. The length L is set by the smallest of three lengths: (b) the wavelength $\lambda = 2\pi/q$, (c) the dynamic length $\gamma/\eta\omega$, and (d) the capillary length ℓ_γ.

we will illustrate the main results pertaining the behavior of the response function in terms of q, Ω, Ca, and θ_0.

V. RESPONSE FUNCTION

We have integrated numerically the equations derived in the previous section. To discuss the results, we wish first to propose a simple interpretation framework that will provide the scaling laws obeyed by the response function $\mathcal{C}$. Let us assume that a perturbation induced at the contact line, in time and/or in space, disturbs the interface over a penetration length L along the plate. For simplicity, we consider a wedge of effective angle θ. From the simple geometrical construction shown in Fig. 2(a), we get for the real part of $\mathcal{C}$, at the linear order in $\hat{\xi}$,

$$R_e(\mathcal{C})\hat{\xi} \equiv \cos(\theta+\theta_1) - \cos\theta \simeq \sin^2\theta\cos\theta\frac{\hat{\xi}}{L}.$$

The viscous force results from the integral over the horizontal direction of the viscous stress. Considering that the fluid moves at the same velocity as the contact line over the wedge region, we obtain the imaginary part of $\mathcal{C}$:

$$I_m(\mathcal{C})\hat{\xi} \propto \frac{3\omega\hat{\xi}\eta}{\gamma\tan\theta}\ln\left(1+\frac{L\tan\theta}{3\ell_s}\right).$$

We therefore predict a relation of the form

$$R_e(\mathcal{C}) \simeq \sin^2\theta\cos\theta\frac{1}{L} \quad \text{and} \quad I_m(\mathcal{C}) \sim \frac{3\omega\eta}{\gamma\tan\theta}\ln\left(1+\frac{L\tan\theta}{3\ell_s}\right),$$

Using the capillary length ℓ_γ to rescale $\mathcal{C}$, we get

$$\ell_\gamma R_e(\mathcal{C}) \simeq \sin^2\theta\cos\theta\frac{\ell_\gamma}{L} \quad \text{and} \quad \ell_\gamma I_m(\mathcal{C}) \sim \frac{3\Omega}{\tan\theta}\ln\left(1+\frac{L\tan\theta}{3\ell_s}\right).$$

In these scaling laws, θ can be considered as the average angle at the scale L, which must scale according to Cox-Voinov law [79]:

$$\theta^3 \sim \theta_0^3 + 9\mathrm{Ca}\ln\left(1+\frac{L\tan\theta_0}{3\ell_s}\right).$$

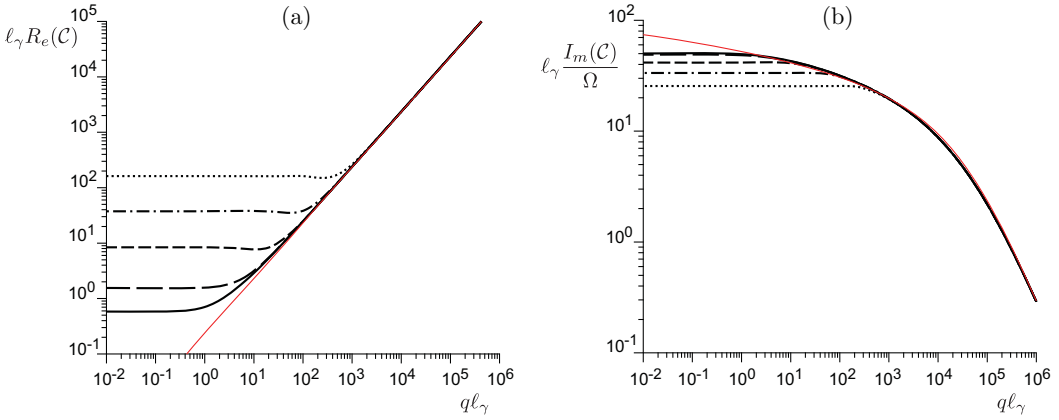

FIG. 3. Response function as a function of the rescaled wave number q, for different values of Ω: $\Omega = 0$ (solid line), $\Omega = 0.22$ (long dashed line), $\Omega = 1$ (dashed line), $\Omega = 4.5$ (dotted dashed line), $\Omega = 20$ (dotted line). The other parameters are fixed at $\tan\theta_0 = 0.55$, $\ell_s = 2.5\times10^{-6}\ell_\gamma$, and $\mathrm{Ca} = 10^{-5}$. The thin red lines are the predictions for the large q asymptotics given by Eq. (32), in which a corrective factor 0.87 was applied in front of the imaginary part.

The logarithmic factor involves the inner cutoff associated with the slip length, which explains that it involves the contact angle θ_0 and not the large-scale angle θ.

The penetration length L depends on three lengths that determine three asymptotic regimes, detailed in the next sections: the perturbation wavelength $\lambda = 2\pi/q$ [Fig. 2(b)], the dynamical length $\gamma/\eta\omega = \ell_\gamma/\Omega$ set by the balance between capillary and viscous effects [Fig. 2(c)], and the capillary length ℓ_γ, which is the outer length of the problem [Fig. 2(d)].

A. Dependence on q

Consider a flat interface which makes an angle θ with the substrate, whose contact line is disturbed with a mode of wave number q. In static conditions, the curvature vanishes so that the interface elevation profile decays as $\sim e^{-|q|x/\cos\theta}$. The disturbance decays exponentially over a penetration length $L = |q|^{-1}\cos\theta$ along the normal x to the contact line. For the real part of the response function (restoring force) we find

$$\gamma\, R_e(\mathcal{C})\hat{\xi} = \gamma\, \sin^2\theta |q| \hat{\xi}.$$

Hence, we obtain

$$\ell_\gamma R_e(\mathcal{C}) = \sin^2\theta|q|\ell_\gamma \quad \text{and} \quad \ell_\gamma I_m(\mathcal{C}) \sim \frac{3\Omega}{\tan\theta} \ln\left(1 + \frac{\cos\theta\tan\theta_0}{3|q|\ell_s}\right). \tag{32}$$

Figure 3 shows the dependence of $\mathcal{C}$ with respect to q for different values of Ω. One observes that the large q regime is independent of Ω (provided Ω is small enough) and nicely coincides with the prediction of a quasistatic disturbance at vanishing curvature. The prediction for $R_e(\mathcal{C})$ is quantitative, but that for $I_m(\mathcal{C})$ is overestimated by $\simeq$13%. A multiplicative factor 0.87 was accordingly applied when plotting the predictions. As expected, $\mathcal{C}$ strongly depends on the (true) contact angle θ_0 in this large q regime (Fig. 4). This dependence is quantitatively predicted by Eq. (32). Finally, Fig. 5 shows that there is a small dependence on the capillary number Ca in this regime, that we interpret as resulting from the change of the interface slope with the scale q^{-1}. As predicted by Eq. (32), the dependence is weak for $I_m(\mathcal{C})$ as the dependence on L is logarithmic, and larger for $R_e(\mathcal{C})$, which linearly depends on L^{-1}. Given the crude assumptions made in the geometrical model, the excellent agreement validates this interpretation.

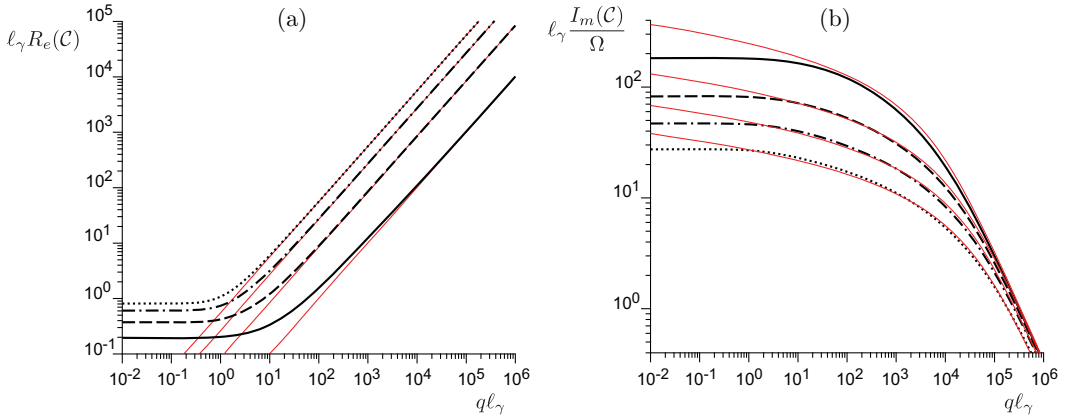

FIG. 4. Response function as a function of the rescaled wave number q, in the limit of vanishing Ω, for different angles $\tan\theta_0$: $\tan\theta_0 = 0.1$ (solid line), $\tan\theta_0 = 0.3$ (dashed line), $\tan\theta_0 = 0.6$ (dotted dashed line), and $\tan\theta_0 = 1.1$ (dotted line). The other parameters are fixed at $\ell_s = 2.5\times10^{-6}\ell_\gamma$, and $\mathrm{Ca} = 10^{-5}$. The thin red lines are the predictions for the large q asymptotics given by Eq. (32), in which a corrective factor 0.87 was applied in front of the imaginary part.

B. Dependence on Ω

Figure 3 shows that there is a crossover at small q between the large q regime discussed above and a regime which depends on the frequency Ω but not on q. Figure 6 shows the dependence on Ω in this small q limit, which presents three asymptotics. In the limit of vanishing Ω, one observes a plateau of $R_e(\mathcal{C})$ while $I_m(\mathcal{C})$ is linear in Ω. This quasisteady asymptotics is discussed in the next section. In the large Ω limit, one observes a power law asymptotics $R_e(\mathcal{C}) = I_m(\mathcal{C}) \propto \Omega^{1/2}$. Finally, in the intermediate asymptotics in Ω, $R_e(\mathcal{C})$ appears to be linear in Ω while $I_m(\mathcal{C})$ is sublinear. This corresponds to the dynamical regime that we now describe, based on the geometrical argument schematized in Fig. 2(c). In the limit of intermediate Ω, the modes penetrate on the interface over a length smaller than the capillary length ℓ_γ but larger than ℓ_s. In order to determine the penetration length L in this case, we can therefore replace the shape of the interface by a wedge at angle θ writing

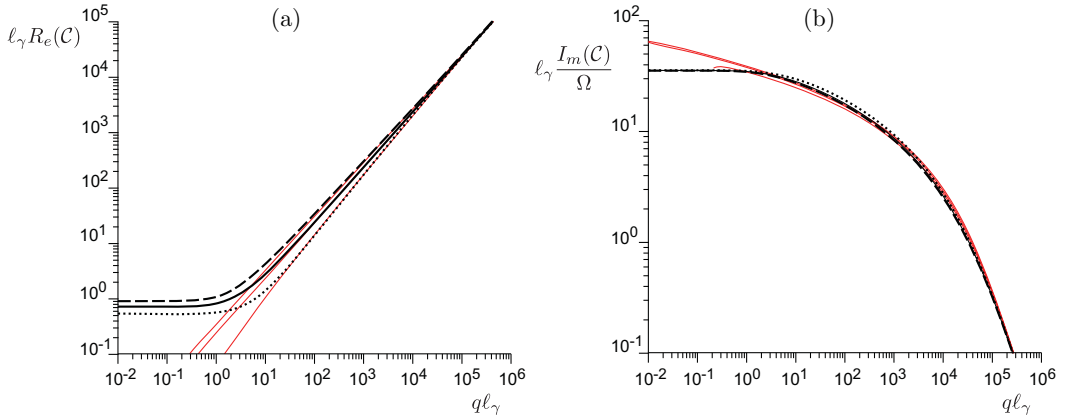

FIG. 5. Response function as a function of the rescaled wave number q, in the limit of vanishing Ω, for different values of Ca: $\mathrm{Ca} = -10^{-3}$ (dotted line), $\mathrm{Ca} = 0$ (solid line), and $\mathrm{Ca} = 10^{-3}$ (dashed line). The other parameters are fixed at $\tan\theta_0 = 0.55$, $\ell_s = 2.5\times10^{-6}\ell_\gamma$. The thin red lines are the predictions for the large q asymptotics given by Eq. (32), in which a corrective factor 0.87 was applied in front of the imaginary part.

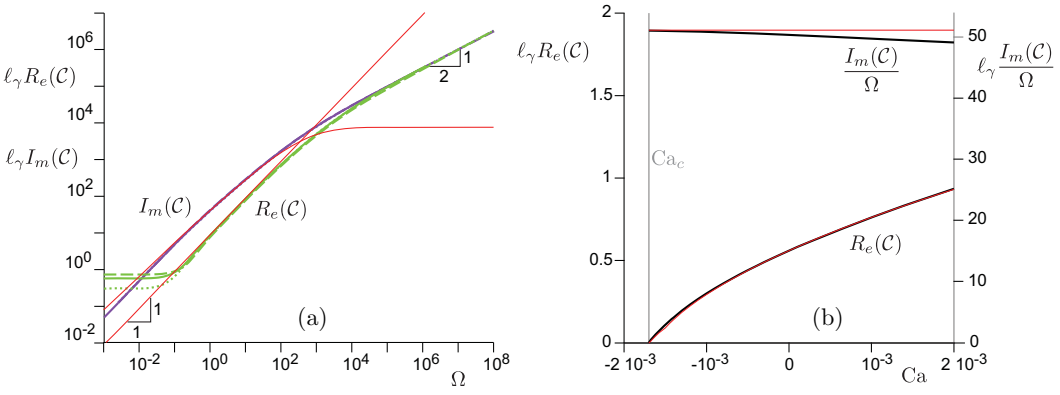

FIG. 6. Left: response function as a function of the rescaled frequency Ω, in the limit of vanishing q, for different values of Ca: $\mathrm{Ca} = -10^{-3}$ (dotted line), $\mathrm{Ca} = 0$ (solid line), and $\mathrm{Ca} = 10^{-3}$ (dashed line). The other parameters are fixed at $\tan\theta_0 = 0.55$, $\ell_s = 2.5\times10^{-6}\ell_\gamma$. The three curves almost collapse for the imaginary part of $\mathcal{C}$ (blue curves) but are split for its real part (green curves), at small Ω. The thin red lines are the predictions of the intermediate asymptotics limited by the dynamical length (small q limit and intermediate range of Ω), as given by Eq. (33). Right: response function in the limit of vanishing Ω and vanishing q, as a function of Ca. The thin red lines are the predictions of the quasisteady asymptotics (small q limit and small Ω), as given by Eq. (34).

$h_0' = \tan\theta$, which leads to the equation:

$$(x^3 h_1''')' = -j\frac{3\Omega}{\ell_\gamma \sin^3\theta} h_1.$$

The above equation presents two independent solutions that converge at infinity (far from the contact line), based on the MeijerG special function [81]. Here we just identify the length L, in its dimensional form, as

$$L \sim \frac{\sin^3\theta\,\ell_\gamma}{3\Omega}.$$

A refined asymptotic treatment gives the multiplicative constants involved in front of L:

$$R_e(\mathcal{C}) \simeq \frac{3\pi\omega\eta}{2\gamma\tan\theta} \quad \text{and} \quad I_m(\mathcal{C}) \sim \frac{3\omega\eta}{\gamma\tan\theta}\ln\left[1 + \frac{\tan\theta_0 \sin^3\theta_0 \ell_\gamma}{3\exp\left(4\gamma_{\mathrm{Euler}} - \frac{1}{2}\right)\Omega\ell_s}\right],$$

where the slip length ℓ_s here has the dimension of a length, and $\gamma_{\mathrm{Euler}} \simeq 0.577$ is the Euler-Mascheroni constant. Rescaling $\mathcal{C}$ by the capillary length, we get

$$\ell_\gamma R_e(\mathcal{C}) \simeq \frac{3\pi\Omega}{2\tan\theta} \quad \text{and} \quad \ell_\gamma I_m(\mathcal{C}) \sim \frac{3\Omega}{\tan\theta}\ln\left[1 + \frac{\tan\theta_0 \sin^3\theta_0 \ell_\gamma}{3\exp\left(4\gamma_{\mathrm{Euler}} - \frac{1}{2}\right)\Omega\ell_s}\right]. \tag{33}$$

The left panel of Fig. 6 shows that the agreement of this model equation with the exact response function is, again, very good in the intermediate range of Ω. The failure appears at large Ω, when the penetration length L reaches the slip length ℓ_s. The large Ω asymptotics is therefore a bit artificial, as the penetration length becomes comparable to the molecular size. This asymptotics is therefore sensitive to the details of the modeling. In order to keep the clarity of the paper, we will not discuss it here. Note that the observed asymptotics $R_e(\mathcal{C}) = I_m(\mathcal{C}) \propto \Omega^{1/2}$ is solution of the Kramers-Kronig relation. At small Ω, the crossover appears when the dynamical length L reaches the outer length ℓ_γ, which sets the size of the meniscus. We discuss this asymptotic in the next section.

C. Dependence on Ca

In the double limit of vanishing Ω and vanishing q, the time evolution is slow and the wavelength much larger than the capillary length. In first approximation, moving the contact line with respect to the plate is the same as moving the plate with respect to the contact line. The main difference lies in the dissipation around the bath. We therefore assume that the dependence of the equilibrium altitude δ with respect to Ca and θ_0 holds during transients, provided one replaces δ by $\delta + \xi$ and Ca by $\mathrm{Ca} + d\xi/dt$ in these laws:

$$\delta = \sqrt{2(1-\sin\theta_M)}\,\ell_\gamma,$$
$$\theta_M^3 = \theta_0^3 + 9\mathrm{Ca}\,\ln\left(\frac{\alpha\ell_\gamma}{3\ell_s}\right).$$

Differentiating these expressions with respect to θ_0, δ, and Ca, one obtains

$$\frac{\theta_0^2}{\sin\theta_0}\ell_\gamma\mathcal{C} = \frac{\theta_M^2\sqrt{2(1-\sin\theta_M)}}{\cos\theta_M} + 3j\Omega\ln\left(\frac{\alpha\ell_\gamma}{3\ell_s}\right). \tag{34}$$

Note that in this expression, we ignored the small dependencies of α with θ_0. The right panel of Fig. 6 shows that the agreement is perfect for the real part of $\mathcal{C}$, as the quasisteady limit is an exact, controlled approximation of the problem for the restoring force. The agreement of the imaginary part of $\mathcal{C}$, which is linear in Ω, is good but not perfect. The approximation used assumes that it is equivalent to impose a displacement of the contact line with respect to the solid plate (the bath remaining fixed) and to impose a displacement of the solid plate with respect to the contact line and the bath. If the small scales of the problem are indeed equivalent and are entirely determined by the relative displacement of the contact line with respect to the plate, the large scales differ if the contact line or the plate move with respect to the bath. The small difference between the prediction and the exact $\mathcal{C}$ results from the small dissipation at the scale of the meniscus.

VI. CONCLUDING REMARKS

The motion of a contact line on a random heterogeneous landscape is one of the most important problems remaining partly open in the field of dynamical wetting [4,7,10–14,17–21,82–84]. Most applications may require only the knowledge of elementary information, e.g., the time evolution of the average contact line position, rather than the complete details of the full problem. In this framework, working in the widely used setup of a plate withdrawal from a bath at a constant velocity [39–42], we have derived the *response function* of the contact line, relating its displacement to the forces set by heterogeneities [cf. Eq. (2)]. To this aim, we have first treated the problem at the hydrodynamic scales, based on the lubrication approximation [48]. Then the space-time evolution of defects' perturbations has been deduced by linearizing the lubrication equations around a base state [80], followed by double Fourier transform in space and time. The dependence of the response function with frequency and wave numbers has then been discussed.

With the response function at hand, several applications can be envisaged. Primarily, one could design a stochastic model accounting for thermal fluctuations, which allows one to study numerically the activated motion of the contact line through the frozen energy landscape provided by defects. Concretely, by using the decomposition

$$\mathcal{C}(q,\omega) = \frac{1}{\ell_\gamma\hat{\phi}_q(\omega)}\left[\hat{\psi}_q(\omega) + j\frac{\eta\ell_\gamma}{\gamma}\omega\right],$$

one could write the following generalized Langevin equation [85]:

$$\eta\frac{d\xi_q}{dt} + \frac{\gamma}{\ell_\gamma}\int_{-\infty}^{t}\psi_q(t-t')\xi_q(t')\,dt' = \int_{-\infty}^{t}\phi_q(t-t')F_q(t')\,dt' + W_q(t), \tag{35}$$

where the subscript q denotes Fourier projection on the qth wave number of the corresponding quantity in real space. Notice that since the system is causal, both $\hat{\psi}_q(\omega)$ and $\hat{\phi}_q(\omega)$ must obey Kramers-Kronig relations (see Ref. [86] and references therein). The term $W_q(t)$ is a stochastic term to be quantified, whose amplitude can be related to the statistical properties of the contact line displacement [61,85]

$$\langle W_q(t) W_q(t')^* \rangle = \eta \langle |\xi_q|^2 \rangle \frac{\gamma}{\ell_\gamma} \psi_q(t - t') \quad (t > t'), \tag{36}$$

where $\langle |\xi_q|^2 \rangle$ needs to be determined to close the problem. On the one hand, $\langle |\xi_q|^2 \rangle$ may be computed by assuming that it results from thermal fluctuations with respect to a static equilibrium ($\Omega \to 0$ and $\mathrm{Ca} \to 0$): this would mean to consider the effects of thermally excited capillary waves damped by gravity at large scale [87]. The problem, however, involves memory kernels and a more complete treatment seems to require the characterization of a "generalized" harmonic energy whose spring constants depend on the response function that we computed in the paper. The equilibration of such energy would then be necessary to obtain $\langle |\xi_q|^2 \rangle$. Work is in progress along this route.

We would remark that this is not the first time that Langevin-type equations have been proposed to quantify the effects of thermal fluctuations on wetting problems at nanoscales. Recent examples include the works in Refs. [25,88], where simplified Langevin dynamics have been used to investigate colloidal dynamics at nonideal interfaces, also with comparisons with molecular dynamics simulations [25]; in Ref. [35] a Langevin-type equation has been used to study the effects of thermal fluctuations on capillary imbibition at nanoscales. A Langevin-type approach has also been used by some of the authors in Ref. [89] to study thermal activation across defects and compare it with experiments. Equation (36) justifies the Langevin approach used in Ref. [89] and further extends it. Indeed, Eqs. (35) involve memory terms, which were not considered in Ref. [89]. Due to these memory terms numerical simulations would require the storage of the contact line profile as a function of time, limiting the possibility for current computers to three or four decades in space.

For instance, the lubrication equations reduce the problem to two dimensions in space and one in time, while the further reduction proposed here leads to one dimension in space and two in time, due to the memory term. The space resolution is fixed by the slip length and the time resolution by visco-capillary velocity γ/η and the slip length. Typical numerical experiments may be performed with 4096 grid points over an integral time (based on the outer length) of order unity. This is not sufficient for direct comparisons with standard laboratory experiments. To reduce the number of decades in actual experiments, one would need to use nanometer-scale-resolved microscopy or to use colloids. An interesting alternative is to test the theory against molecular dynamic simulations, which have very similar constraints in terms of space and timescales. With the precise determination of the noise in hand, the natural follow-up would be to perform side-by-side comparisons between the outcome of experiments and the prediction of the stochastic model. This requires the experimental determination of the energy landscape of a well-controlled heterogeneous substrate and experimental visualization of the contact line at the nanoscales. As the model is derived in the linear response regime, this opens the question, beside technical difficulties, of possible nonlinear effects. Another interesting follow-up would be the study of (35) in the presence of an external driving mechanism periodically oscillating in time. This can be used to analyze the phenomenon of stochastic resonance [90,91], by studying the interplay between the characteristic hopping timescale set by thermal activation and the external timescale set by the periodic driving.

Finally, we wish to remark that the framework derived in this paper opens the promising perspective of treating the mechanical behavior of a contact line, its "rheology," using low-dimensional models [92–98]. It directly connects to current progresses in soft-glassy materials [99], which shares strong similarities with the contact line problem: the multiscale character, the presence of a dynamic critical point, and a self-built energy landscape. Controlled reductions to low-dimensional models may help to

overcome the intrinsic limit of the formulation derived here (linear response, a well-known large-scale asymptotics). A potential application is to solve the inverse problem and to determine mechanical and chemical properties of an interface using a contact line. Such a contact line nano-rheometer would be particularly interesting in the case of soft solids, with direct applications on bio-medical tissues.

ACKNOWLEDGMENTS

B.A. is supported by Institut Universitaire de France (IUF). This work was funded by the Agence Nationale de la Recherche (ANR) grant Smart.

H.P. and D.B. have contributed equally to this work.

APPENDIX: BOUNDARY CONDITIONS AND ASYMPTOTICS AT THE PLATE

Let us introduce the following formulation:

$$h(x,y,t) = h_0(x-\xi) + \tilde{h}_1(x-\xi)e^{j\Omega t+jqy},$$

where (the real part of) $\xi = \hat{\xi}e^{j\Omega t+jqy}$ parametrizes the disturbance to the contact line position for given frequency Ω and wave number q. The boundary conditions are

$$\begin{aligned} h(\xi,y,t) &= 0, \\ \partial_x h(\xi,y,t) &= \tan\theta_Y(y,t) \simeq \tan\theta_0 + \left.\frac{d\tan\theta}{d\theta}\right|_{\theta=\theta_0} \theta_1(y,t), \\ \mathcal{F}(\xi,y,t) &= 0. \end{aligned}$$

Note that the contact angle is normally taken along the normal to the contact line. However, as the base state is invariant along the y direction, the normal is along x within negligible quadratic disturbances, hence the above expressions. We see that the description in terms of the displaced variable $x-\xi$ is perfectly well behaved. The linear equations giving $\tilde{h}_1$ are entirely equivalent to those giving h_1. $\tilde{h}_1$ is totally equivalent to h_1, at the linear order (but not at the nonlinear order). We shall therefore use h_1, which leads to simpler equations, but keep in mind that we will actually represent the solution by $\tilde{h}_1$. The equivalence is given by the following equations:

$$h_0(x) + h_1(x)e^{j\Omega t+jqy} = h(x,t) \simeq h_0(x) - \xi h_0'(x) + \tilde{h}_1(x)e^{j\Omega t+jqy},$$

from which we get

$$\tilde{h}_1(x) = h_1(x) + \hat{\xi}h_0'(x).$$

Therefore, based on (3), we get the boundary conditions (25)–(27). Note that, as the system is linear, the solution is independent of the amplitude of the disturbance, so that $\hat{\xi}$ has been set to unity without loss of generality.

As explained in the main text, we then derive the general asymptotics at the plate. Let us introduce the following shorthand notations:

$$t_0 = \tan\theta_0, \quad s_0 = \sin\theta_0, \quad c_0 = \cos\theta_0 = \left(1+t_0^2\right)^{-1/2}.$$

By keeping vanishing the zeroth order (in x) of the asymptotic solution $\mathcal{X}$ except for its h_1 component, we get

$$\mathcal{X}_h = \begin{pmatrix} 1 - \frac{\mathrm{Ca}}{\ell_s s_0^2 c_0} x \ln\left(\frac{x}{\ell}\right) + \frac{\mathrm{Ca}}{\ell_s s_0^2 c_0} x + \frac{3\mathrm{Ca}^2}{2\ell_s^2 s_0^2 c_0^2} x^2 \ln^2\left(\frac{x}{\ell}\right) - \left(3 + \frac{1}{4s_0^2}\right) \frac{\mathrm{Ca}^2}{\ell_s^2 s_0^2 c_0^2} x^2 \ln\left(\frac{x}{\ell}\right) \\ + \left[\frac{q^2}{2c_0^2} + \left(1 + \frac{1}{4s_0^2}\right) \frac{3\mathrm{Ca}^2}{2\ell_s^2 s_0^2 c_0^2}\right] x^2 + O(x^3 \ln^3 x) \\ - \frac{\mathrm{Ca}}{\ell_s s_0^2 c_0} \ln\left(\frac{x}{\ell}\right) + \frac{3\mathrm{Ca}^2}{\ell_s^2 s_0^2 c_0^2} x \ln^2\left(\frac{x}{\ell}\right) - \left(3 + \frac{1}{2s_0^2}\right) \frac{\mathrm{Ca}^2}{\ell_s^2 s_0^2 c_0^2} x \ln\left(\frac{x}{\ell}\right) + \left(\frac{q^2}{c_0^2} + \frac{\mathrm{Ca}^2}{2\ell_s^2 s_0^4 c_0^2}\right) x + O(x^2 \ln^3 x) \\ - \frac{\mathrm{Ca}}{\ell_s t_0^2} x^{-1} - \frac{\mathrm{Ca}^2 c_0}{2\ell_s^2 s_0^4} \ln\left(\frac{x}{\ell}\right) + O(x \ln^2 x) \\ - \frac{q^2 \mathrm{Ca}}{2} x^2 + \left(\frac{q^2 \mathrm{Ca}^2}{6\ell_s s_0^2 c_0} - \frac{\Omega^2}{6\ell_s s_0^2 c_0}\right) x^3 \ln\left(\frac{x}{\ell}\right) + \left(\frac{11\Omega^2}{36\ell_s s_0^2 c_0} - \frac{q^2 \mathrm{Ca}\, s_0}{9\ell_s c_0^4} - \frac{5q^2 \mathrm{Ca}^2}{9\ell_s s_0^2 c_0}\right) x^3 + O(x^4 \ln^2 x) \end{pmatrix}$$

$$- j\Omega \begin{pmatrix} \frac{1}{2\ell_s s_0^2 c_0} x^2 \ln\left(\frac{x}{\ell}\right) - \frac{3}{4\ell_s s_0^2 c_0} x^2 + O(x^3 \ln^2 x) \\ \frac{1}{\ell_s s_0^2 c_0} x \ln\left(\frac{x}{\ell}\right) - \frac{1}{\ell_s s_0^2 c_0} x + O(x^2 \ln^2 x) \\ \frac{1}{\ell_s t_0^2} \ln\left(\frac{x}{\ell}\right) + O(x \ln x) \\ x - \frac{\mathrm{Ca}}{2\ell_s s_0^2 c_0} x^2 \ln\left(\frac{x}{\ell}\right) + \frac{3\mathrm{Ca}}{4\ell_s s_0^2 c_0} x^2 + \frac{\mathrm{Ca}^2}{2\ell_s^2 s_0^2 c_0^2} x^3 \ln^2\left(\frac{x}{\ell}\right) + \left[\frac{q^2}{3} - \left(4 + \frac{1}{4s_0^2}\right) \frac{\mathrm{Ca}^2}{3\ell_s^2 s_0^2 c_0^2}\right] x^3 \ln\left(\frac{x}{\ell}\right) \\ + \left[\left(\frac{3}{2c_0^2} - 1\right) \frac{q^2}{9} + \left(17 + \frac{11}{4s_0^2}\right) \frac{\mathrm{Ca}^2}{18\ell_s^2 s_0^2 c_0^2}\right] x^3 + O(x^4 \ln^3 x) \end{pmatrix}.$$

By keeping vanishing the zeroth order of $\mathcal{X}$ except for its h_1' component, we get

$$\mathcal{X}_\theta = \begin{pmatrix} x + \left(\frac{1}{t_0^2} - 2\right) \frac{\mathrm{Ca}}{2\ell_s c_0} x^2 \ln\left(\frac{x}{\ell}\right) + \left(2 - \frac{1}{t_0^2}\right) \frac{3\mathrm{Ca}}{4\ell_s c_0} x^2 + O(x^3 \ln^2 x) \\ 1 + \left(\frac{1}{t_0^2} - 2\right) \frac{\mathrm{Ca}}{\ell_s c_0} x \ln\left(\frac{x}{\ell}\right) + \left(2 - \frac{1}{t_0^2}\right) \frac{\mathrm{Ca}}{\ell_s c_0} x + O(x^2 \ln^2 x) \\ \frac{\mathrm{Ca}}{\ell_s t_0^2} \ln\left(\frac{x}{\ell}\right) + O(x \ln^2 x) \\ \frac{q^2 \mathrm{Ca}}{3} x^3 \ln\left(\frac{x}{\ell}\right) - \frac{q^2 \mathrm{Ca}}{9} x^3 + O(x^4 \ln^2 x) \end{pmatrix}$$

$$- j\Omega \begin{pmatrix} O(x^3 \ln^2 x) \\ O(x^2 \ln^2 x) \\ O(x \ln x) \\ \frac{1}{2} x^2 + \left(\frac{1}{t_0^2} - 2\right) \frac{\mathrm{Ca}}{6\ell_s c_0} x^3 \ln\left(\frac{x}{\ell}\right) + \left(2 - \frac{1}{t_0^2}\right) \frac{11\mathrm{Ca}}{36\ell_s c_0} x^3 + O(x^4 \ln^2 x) \end{pmatrix}.$$

By keeping vanishing the zeroth order of $\mathcal{X}$ except for its κ_1 component, we get

$$\mathcal{X}_\kappa = \begin{pmatrix} \frac{1}{2c_0^3} x^2 + O(x^3 \ln^2 x) \\ \frac{1}{c_0^3} x + O(x^2 \ln^2 x) \\ 1 + O(x \ln^2 x) \\ \frac{q^2 \ell_s t_0^2}{3} x^3 + O(x^4 \ln^2 x) \end{pmatrix} - j\Omega \begin{pmatrix} o(x^3 \ln^2 x) \\ o(x^2 \ln^2 x) \\ o(x \ln x) \\ \frac{1}{6c_0^3} x^3 + O(x^4 \ln^2 x) \end{pmatrix}.$$

We do not report the analogous asymptotic having the zeroth order of the $\mathcal{F}_1$ component of $\mathcal{X}$ nonvanishing as it is unphysical (the flux must vanish at the contact line).

[1] P.-G. de Gennes, Wetting: Statics and dynamics, Rev. Mod. Phys. **57**, 827 (1985).

[2] P.-G. de Gennes, F. Brochard-Wyart, and D. Quere, *Capillarity and Wetting Phenomena: Drops, Bubbles, Pearls, Waves* (Springer, New York, 2013).

[3] M. Rauscher and S. Dietrich, Wetting phenomena in nanofluidics, Annu. Rev. Mater. Res. **38**, 143 (2008).

[4] D. Bonn, J. Eggers, J. Indekeu, J. Meunier, and E. Rolley, Wetting and spreading, Rev. Mod. Phys. **81**, 739 (2009).
[5] D. Wasan, A. Nikolov, and K. Kondiparty, The wetting and spreading of nanofluids on solids: Role of the structural disjoining pressure, Curr. Opin. Colloid Interface Sci. **16**, 344 (2011).
[6] M. N. Popescu, G. Oshanin, S. Dietrich, and A.-M. Cazabat, Precursor films in wetting phenomena, J. Phys.: Condens. Matter **24**, 243102 (2012).
[7] J. H. Snoeijer and B. Andreotti, Moving contact lines: Scales, regimes, and dynamical transitions, Annu. Rev. Fluid Mech. **45**, 269 (2013).
[8] J. Wang, M. Do-Quang, J. J. Cannon, F. Yue, Y. Suzuki, G. Amberg, and J. Shiomi, Surface structure determines dynamic wetting, Sci. Rep. **5**, 8474 (2015).
[9] R. Raj, S. Adera, R. Enright, and E. N. Wang, High-resolution liquid patterns via three-dimensional droplet shape control, Nat. Commun. **5**, 4975 (2014).
[10] H.-M. Kwon, J. C. Bird, and K. K. Varanasi, Increasing Leidenfrost point using micro-nano hierarchical surface structures, Appl. Phys. Lett. **103**, 201601 (2013).
[11] H. Sirringhaus, T. Kawase, R. H. Friend, T. Shimoda, M. Inbasekaran, W. Wu, and E. P. Woo, High-resolution inkjet printing of all-polymer transistor circuits, Science **290**, 2123 (2000).
[12] T. H. J. van Osch, J. Perelaer, A. W. M. de Laat, and U. S. Schubert, Inkjet printing of narrow conductive tracks on untreated polymeric substrates, Adv. Mater. **20**, 343 (2008).
[13] B. Y. Ahn, E. B. Duoss, M. J. Motala, X. Guo, S.-I. Park, Y. Xiong, J. Yoon, R. G. Nuzzo, J. A. Rogers, and J. A. Lewis, Omnidirectional printing of flexible, stretchable, and spanning silver microelectrodes, Science **323**, 1590 (2009).
[14] M. S. Onses, C. Song, L. Williamson, E. Sutanto, P. M. Ferreira, A. G. Alleyne, P. F. Nealey, H. Ahn, and J. A. Rogers, Hierarchical patterns of three-dimensional block-copolymer films formed by electrohydrodynamic jet printing and self-assembly, Nat. Nanotechnol. **8**, 667 (2013).
[15] M. Sbragaglia, A. M. Peters, C. Pirat, B. M. Borkent, R. G. H. Lammertink, M. Wessling, and D. Lohse, Spontaneous Breakdown of Superhydrophobicity, Phys. Rev. Lett. **99**, 156001 (2007).
[16] S. Adera, R. Raj, R. Enright, and E. N. Wang, Non-wetting droplets on hot superhydrophilic surfaces, Nat. Commun. **4**, 2518 (2013).
[17] J. C. Bird, R. Dhiman, H.-M. Kwon, and K. K. Varanasi, Reducing the contact time of a bouncing drop, Nature (London) **503**, 385 (2013).
[18] Y. Liu, L. Moevius, X. Xu, T. Qian, J. M. Yeomans, and Z. Wang, Pancake bouncing on superhydrophobic surfaces, Nat. Phys. **10**, 515 (2014).
[19] J.-U. Park, M. Hardy, S. J. Kang, K. Barton, K. Adair, D. K. Mukhopadhyay, C. Y. Lee, M. S. Strano, A. G. Alleyne, J. G. Georgiadis, P. M. Ferreira, and J. A. Rogers, High-resolution electrohydrodynamic jet printing, Nat. Mater. **6**, 782 (2007).
[20] C. Duprat, S. Protière, A. Beebe, and H. Stone, Wetting of flexible fibre arrays, Nature (London) **482**, 510 (2012).
[21] A. T. Paxson and K. K. Varanasi, Self-similarity of contact line depinning from textured surfaces, Nat. Commun. **4**, 1492 (2013).
[22] H. Lehle, M. Oettel, and S. Dietrich, Effective forces between colloids at interfaces induced by capillary wavelike fluctuations, Europhys. Lett. **75**, 174 (2006).
[23] T. Bickel, Probing nanoscale deformations of a fluctuating interface, Europhys. Lett. **106**, 16004 (2014).
[24] G. Boniello, C. Blanc, D. Fedorenko, M. Medfai, N. B. Mbarek, M. In, M. Gross, A. Stocco, and M. Nobili, Brownian diffusion of a partially wetted colloid, Nat. Mater. **14**, 908 (2015).
[25] C. E. Colosqui, J. F. Morris, and J. Koplik, Colloidal Adsorption at Fluid Interfaces: Regime Crossover from Fast Relaxation to Physical Aging, Phys. Rev. Lett. **111**, 028302 (2013).
[26] A. M. Rahmani, A. Wang, V. N. Manoharan, and C. E. Colosqui, Colloidal particle adsorption at liquid interfaces: Capillary driven dynamics and thermally activated kinetics, Soft Matter **12**, 6365 (2016).
[27] A. Wang, W. B. Rogers, and V. N. Manoharan, Effects of Contact-Line Pinning on the Adsorption of Nonspherical Colloids at Liquid Interfaces, Phys. Rev. Lett. **119**, 108004 (2017).
[28] J. Koplik and C. Maldarelli, Diffusivity and hydrodynamic drag of nanoparticles at a vapor-liquid interface, Phys. Rev. Fluids **2**, 024303 (2017).

[29] A. Moosavi, M. Rauscher, and S. Dietrich, Size dependent motion of nanodroplets on chemical steps, J. Chem. Phys. **129**, 044706 (2008).
[30] A. Moosavi, M. Rauscher, and S. Dietrich, Motion of nanodroplets near chemical heterogeneities, Langmuir **24**, 734 (2008).
[31] M. Rauscher and S. Dietrich, Nano-droplets on structured substrates, Soft Matter **5**, 2997 (2009).
[32] B. Davidovitch, E. Moro, and H. A. Stone, Spreading of Viscous Fluid Drops on a Solid Substrate Assisted by Thermal Fluctuations, Phys. Rev. Lett. **95**, 244505 (2005).
[33] S. Nesic, R. Cuerno, E. Moro, and L. Kondic, Dynamics of thin fluid films controlled by thermal fluctuations, Eur. Phys. J. Special Topics **224**, 379 (2015).
[34] C. E. Colosqui, T. Teng, and A. M. Rahmani, Wetting Driven by Thermal Fluctuations on Terraced Nanostructures, Phys. Rev. Lett. **115**, 154504 (2015).
[35] C. E. Colosqui, J. S. Wexler, Y. Liu, and H. A. Stone, Crossover from shear-driven to thermally activated drainage of liquid-infused microscale capillaries, Phys. Rev. Fluids **1**, 064101 (2016).
[36] A. Giacomello, L. Schimmele, and S. Dietrich, Wetting hysteresis induced by nanodefects, Proc. Natl. Acad. Sci. USA **113**, E262 (2016).
[37] A. Giacomello, S. Meloni, M. Chinappi, and C. M. Casciola, Cassie-Baxter and Wenzel states on a nanostructured surface: Phase diagram, metastabilities, and transition mechanism by atomistic free energy calculations, Langmuir **28**, 10764 (2012).
[38] A. Giacomello, M. Chinappi, S. Meloni, and C. M. Casciola, Metastable Wetting on Superhydrophobic Surfaces: Continuum and Atomistic Views of the Cassie-Baxter-Wenzel Transition, Phys. Rev. Lett. **109**, 226102 (2012).
[39] J. Eggers, Hydrodynamic Theory of Forced Dewetting, Phys. Rev. Lett. **93**, 094502 (2004).
[40] J. Eggers, Existence of receding and advancing contact lines, Phys. Fluids **17**, 082106 (2005).
[41] J. Eggers, Contact line motion for partially wetting fluids, Phys. Rev. E **72**, 061605 (2005).
[42] T. S. Chan, J. H. Snoeijer, and J. Eggers, Theory of the forced wetting transition, Phys. Fluids **24**, 072104 (2012).
[43] J. H. Snoeijer and B. Andreotti, A microscopic view on contact angle selection, Phys. Fluids **20**, 057101 (2008).
[44] D. Seveno, T. D. Blake, and J. De Coninck, Young's Equation at the Nanoscale, Phys. Rev. Lett. **111**, 096101 (2013).
[45] B. Dai, L. G. Leal, and A. Redondo, Disjoining pressure for nonuniform thin films, Phys. Rev. E **78**, 061602 (2008).
[46] A. A. Pahlavan, L. Cueto-Felgueroso, G. H. McKinley, and R. Juanes, Thin Films in Partial Wetting: Internal Selection of Contact-Line Dynamics, Phys. Rev. Lett. **115**, 034502 (2015).
[47] C. Huh and L. E. Scriven, Hydrodynamic model of steady movement of a solid/liquid/fluid contact line, J. Colloid Interface Sci. **35**, 85 (1971).
[48] A. Oron, S. H. Davis, and S. G. Bankoff, Long-scale evolution of thin liquid films, Rev. Mod. Phys. **69**, 931 (1997).
[49] A. Prevost, E. Rolley, and C. Guthmann, Thermally Activated Motion of the Contact Line of a Liquid Helium-4 Meniscus on a Cesium Substrate, Phys. Rev. Lett. **83**, 348 (1999).
[50] L. D. Landau and E. M. Lifshitz, *Fluid Mechanics* (Pergamon Press, London, 1959).
[51] E. G. Flekkøy and D. H. Rothman, Fluctuating hydrodynamic interfaces: Theory and simulation, Phys. Rev. E **53**, 1622 (1996).
[52] J. M. O. De Zarate and J. V. Sengers, *Hydrodynamic Fluctuations in Fluids and Fluid Mixtures* (Elsevier, Amsterdam, 2006).
[53] G. Grün, K. Mecke, and M. Rauscher, Thin-film flow influenced by thermal noise, J. Stat. Phys. **122**, 1261 (2006).
[54] D. Belardinelli, M. Sbragaglia, M. Gross, and B. Andreotti, Thermal fluctuations of an interface near a contact line, Phys. Rev. E **94**, 052803 (2016).
[55] M. A. Durán-Olivencia, R. S. Gvalani, S. Kalliadasis, and G. A. Pavliotis, Instability, rupture and fluctuations in thin liquid films: Theory and computations, arXiv:1707.08811 (2017).

[56] S. Nesic, R. Cuerno, E. Moro, and L. Kondic, Fully nonlinear dynamics of stochastic thin-film dewetting, Phys. Rev. E **92**, 061002(R) (2015).
[57] M. E. Fisher, Walks, walls, wetting, and melting, J. Stat. Phys. **34**, 667 (1984).
[58] J. Bricmont, A. El Mellouki, and J. Fröhlich, Random surfaces in statistical mechanics: Roughening, rounding, wetting, J. Stat. Phys. **42**, 743 (1986).
[59] J. L. Lebowitz and C. Maes, The effect of an external field on an interface, entropic repulsion, J. Stat. Phys. **46**, 39 (1987).
[60] J. Crassous and E. Charlaix, Contact angle hysteresis on a heterogeneous surface: Solution in the limit of a weakly distorted contact line, Europhys. Lett. **28**, 415 (1994).
[61] P. Hänggi, P. Talkner, and M. Borkovec, Reaction-rate theory: Fifty years after Kramers, Rev. Mod. Phys. **62**, 251 (1990).
[62] J. F. Joanny and P.-G. De Gennes, A model for contact angle hysteresis, J. Chem. Phys. **81**, 552 (1984).
[63] C. Bauer and S. Dietrich, Quantitative study of laterally inhomogeneous wetting films, Eur. Phys. J. B **10**, 767 (1999).
[64] T. Getta and S. Dietrich, Line tension between fluid phases and a substrate, Phys. Rev. E **57**, 655 (1998).
[65] G. J. Merchant and J. B. Keller, Contact angles, Phys. Fluids A **4**, 477 (1992).
[66] J. Weijs, A. Marchand, B. Andreotti, D. Lohse, and J. H. Snoeijer, Origin of line tension for a Lennard-Jones nanodroplet, Phys. Fluids **23**, 022001 (2011).
[67] A. Marchand, J. H. Weijs, J. H. Snoeijer, and B. Andreotti, Why is surface tension a force parallel to the interface? Am. J. Phys. **79**, 999 (2011).
[68] M. Horsch, H. Hasse, A. K. Shchekin, A. Agarwal, S. Eckelsbach, J. Vrabec, E. A. Müller, and G. Jackson, Excess equimolar radius of liquid drops, Phys. Rev. E **85**, 031605 (2012).
[69] A. Tröster, M. Oettel, B. Block, P. Virnau, and K. Binder, Numerical approaches to determine the interface tension of curved interfaces from free energy calculations, J. Chem. Phys. **136**, 064709 (2012).
[70] M. H. Factorovich, V. Molinero, and D. A. Scherlis, Vapor pressure of water nanodroplets, J. Am. Chem. Soc. **136**, 4508 (2014).
[71] M. N. Joswiak, N. Duff, M. F. Doherty, and B. Peters, Size-dependent surface free energy and Tolman-corrected droplet nucleation of TIP4P/2005 water, J. Phys. Chem. Lett. **4**, 4267 (2013).
[72] N. Bruot and F. Caupin, Curvature Dependence of the Liquid-Vapor Surface Tension Beyond the Tolman Approximation, Phys. Rev. Lett. **116**, 056102 (2016).
[73] L. Schimmele, M. Napiorkowski, and S. Dietrich, Conceptual aspects of line tensions, J. Chem. Phys. **127**, 164715 (2007).
[74] L. Schimmele and S. Dietrich, Line tension and the shape of nanodroplets, Eur. Phys. J. E **30**, 427 (2009).
[75] J. Indekeu, Line tension at wetting, Int. J. Mod. Phys. B **8**, 309 (1994).
[76] J. Drelich and J. D. Miller, The effect of solid surface heterogeneity and roughness on the contact angle/drop (bubble) size relationship, J. Colloid Interface Sci. **164**, 252 (1994).
[77] J. Drelich and J. Miller, The line/pseudo-line tension in three-phase systems, Particul. Sci. Technol. **10**, 1 (1992).
[78] J. Gaydos and A. Neumann, The dependence of contact angles on drop size and line tension, J. Colloid Interface Sci. **120**, 76 (1987).
[79] O. V. Voinov, Hydrodynamics of wetting, Fluid Dyn. **11**, 714 (1976).
[80] J. H. Snoeijer, B. Andreotti, G. Delon, and M. Fermigier, Relaxation of a dewetting contact line. Part 1. A full-scale hydrodynamic calculation, J. Fluid. Mech. **579**, 63 (2007).
[81] I. S. Gradshteyn and I. M. Ryzhik, *Table of Integrals, Series, and Products* (Academic Press, New York, 2014).
[82] H. Fan, Y. Lu, A. Stump, S. T. Reed, T. Baer, R. Schunk, V. Perez-Luna, G. P. López, and C. J. Brinker, Rapid prototyping of patterned functional nanostructures, Nature (London) **405**, 56 (2000).
[83] M. A. C. Stuart, W. T. S. Huck, J. Genzer, M. Müller, C. Ober, M. Stamm, G. B. Sukhorukov, I. Szleifer, V. V. Tsukruk, M. Urban, F. Winnik, S. Zauscher, I. Luzinov, and S. Minko, Emerging applications of stimuli-responsive polymer materials, Nat. Mater. **9**, 101 (2010).
[84] P. Galliker, J. Schneider, H. Eghlidi, S. Kress, V. Sandoghdar, and D. Poulikakos, Direct printing of nanostructures by electrostatic autofocussing of ink nanodroplets, Nat. Commun. **3**, 890 (2012).

[85] R. Kubo, The fluctuation-dissipation theorem, Rep. Prog. Phys. **29**, 255 (1966).
[86] J. S. Toll, Causality and the dispersion relation: Logical foundations, Phys. Rev. **104**, 1760 (1956).
[87] S. A. Safran, *Statistical Thermodynamics of Surfaces, Interfaces, and Membranes* (Westview Press, Boulder, 2003).
[88] J. de Graaf, M. Dijkstra, and A. van Roij, Adsorption trajectories and free-energy separatrices for colloidal particles in contact with a liquid-liquid interface, J. Chem. Phys. **132**, 164902 (2010).
[89] H. Perrin, R. Lhermerout, K. Davitt, E. Rolley, and B. Andreotti, Defects at the Nanoscale Impact Contact Line Motion at all Scales, Phys. Rev. Lett. **116**, 184502 (2016).
[90] R. Benzi, A. Sutera, and A. Vulpiani, The mechanism of stochastic resonance, J. Phys. A **14**, L453 (1981).
[91] L. Gammaitoni, P. Hänggi, P. Jung, and F. Marchesoni, Stochastic resonance, Rev. Mod. Phys. **70**, 223 (1998).
[92] K. Martens, L. Bocquet, and J.-L. Barrat, Spontaneous formation of permanent shear bands in a mesoscopic model of flowing disordered matter, Soft Matter **8**, 4197 (2012).
[93] V. Mansard, A. Colin, P. Chauduri, and L. Bocquet, A kinetic elasto-plastic model exhibiting viscosity bifurcation in soft glassy materials, Soft Matter **7**, 5524 (2011).
[94] G. Picard, A. Ajdari, L. Bocquet, and F. Lequeux, Simple model for heterogeneous flows of yield stress fluids, Phys. Rev. E **66**, 051501 (2002).
[95] P. Hébraud and F. Lequeux, Mode-Coupling Theory for the Pasty Rheology of Soft Glassy Materials, Phys. Rev. Lett. **81**, 2934 (1998).
[96] P. Sollich, F. Lequeux, P. Hébraud, and M. E. Cates, Rheology of Soft Glassy Materials, Phys. Rev. Lett. **78**, 2020 (1997).
[97] P. Sollich, Rheological constitutive equation for a model of soft glassy materials, Phys. Rev. E **58**, 738 (1998).
[98] P. Sollich and M. E. Cates, Thermodynamic interpretation of soft glassy rheology models, Phys. Rev. E **85**, 031127 (2012).
[99] D. Bonn, M. M. Denn, L. Berthier, T. Divoux, and S. Manneville, Yield stress materials in soft condensed matter, Rev. Mod. Phys. **89**, 035005 (2017).